Bulgarian Journal of Physics vol. **51** (2024) 311–338

Calculating the Absorption Edge of Thin Films

Aarne Kasikov*, **Lauri Aarik**

Institute of Physics, University of Tartu, W. Ostwaldi 1, 50411 Tartu, Estonia
*Corresponding author E-mail: aarnek@ut.ee

Received: 6 January 2023
doi: https://doi.org/10.55318/bgjp.2024.51.4.311

Abstract. The position of the absorption edge (the energy where the absorption values begin to differ from zero) is one of the often used characteristics of the material. For thin films, it is usually obtained from transmission or transmission and reflection values of the film using different approximate methods and models to simplify the analysis. A reason for this is that the transmittance and reflectance of the film samples depend not only on the absorption but also on the interference inside a film and on the reflection from the backside of a transparent substrate. For bulk material and thicker films, the interference effects can be ignored, but for films thinner than 1 μm, it can create a real problem. In this study we present the results obtained using the different mathematical approaches to calculate absorption coefficient of a model film and analyze the applicability of these methods. The absorption edge of the atomic layer deposited $Hf_xTi_yO_z$ films using different approximations is calculated and the amount of scattering of resulting values caused by different calculation methods is demonstrated. According to our study, the most appropriate model is the one presented by W.Q. Hong.

KEY WORDS: thin film, absorption edge, absorption coefficient, transmittance, reflectance, ALD, ellipsometry, hafnium titanate.

1 Introduction

The absorption edge of materials is typically defined as a threshold at which the absorption coefficient

$$\alpha = 4\pi k/\lambda \tag{1}$$

reaches zero. Here, the k is an absorption index (imaginary part of the complex refractive index) and λ is the wavelength. The absorption edge quantifies the lowest radiation energy that a material absorbs. Depending on the nature of the absorption processes, the absorption coefficient dependence on photon energy in classical approach can be given as

$$\alpha = A_1 (h\nu - E_g)^{1/2} \tag{2}$$

1310–0157 © 2024 Union of the Physicists in Bulgaria (UPB)

for direct transitions (without the assistance of phonons),

$$\alpha = A_2 \frac{(h\nu - E_g + E_p)^2}{\exp(E_p/kT) - 1} \tag{3}$$

for indirect transitions with the absorption of phonons,

$$\alpha = A_3 \exp(h\nu/E_0) \tag{4}$$

for transitions between band tails (the Urbach tail), or something else [1, pp. 34-46]. Here, E_g is the value of the absorption edge and E_p is the energy of the phonon participating in the absorption process.

The dependence of absorption coefficient on photon energy is transformed to a linear scale as

$$\alpha^2 = A_4(h\nu - E_g) \tag{5}$$

for direct transitions and

$$\alpha^{1/2} = A_5\,(h\nu - E_g) \tag{6}$$

for indirect transitions if the temperature dependence of the absorption and the transitions with phonon emission are not considered. For Urbach tail caused by impurity and defect states near zone edges, absorption can be presented as linear at semilogarithmic plot.

These dependencies of absorption on photon energy represent the physical processes in the material induced by light absorption. To understand which processes take place at absorption for particular materials, we need to determine the absorption coefficient for different wavelengths.

For bulk material, a well-known Beer-Lambert law (hereafter referred to as the Lambert law) describes the adsorption as

$$I = I_0 e^{-\alpha z}\,, \tag{7}$$

where I is the light intensity, I_0 is the incident light intensity, and z is the path length. Here, material homogeneity, scattering, absorption nonlinearity, and other effects are not considered. However, scattering in bulk material caused by the structural inhomogeneities introduces additional losses in the transmitted radiation. All those losses can formally be added to the absorption, as the scattered light is lost for a straight beam of light. However, nonlinearity can only be excluded if the incident light intensity is low. If the material is sufficiently thick to avoid the interference effects in a slab, the losses from reflections on the surfaces where light enters and leaves the material can also be added into the formula, as

$$I = I_0 T e^{-\alpha z} T = (1 - R)^2 I_0 e^{-\alpha z}\,. \tag{8}$$

Here, R and T are the reflection and transmission coefficients of one surface of the sample under normal incidence and at a given wavelength. If two plates with parallel faces and different thicknesses are considered, we get

$$I_1 = I_0 e^{-\alpha z_1}\,, \qquad I_2 = I_0 e^{-\alpha z_2} \tag{9}$$

with a possibility to exclude the incident light intensity and the reflection losses as

$$I_2/I_1 = e^{-\alpha(z_2 - z_1)}\,. \tag{10}$$

For case of a thin film, the situation is more complicated owing to the interference in the film and reflectance from the rear face of the substrate. The interference introduces additional modulation into measured spectrophotometric spectra and influences the results. Therefore, to obtain the real absorption value, these effects need to be separated.

The simplest method for this comprises ignoring both the interference within the film and reflectance from the substrates rear face. In this case, intensity is defined as in (7), then

$$I/I_0 = e^{-\alpha z} = T\,, \quad \text{and} \quad \alpha d = \ln(1/T)\,. \tag{11}$$

Here, z equals the film thickness d. However, the film thickness has to be determined using a different method as it is not known. Thus, optical density αd can be used instead of film thickness for characterizing a particular sample. Optical density (absorbance), in this formula denoted by $1/T$, has several different definitions. In our study, it is a parameter of a material though being dependent on film thickness. Its value will depend on the method that is used to determine it. Although optical density of films varies with their thickness, the absorption coefficient α of the material should remain approximately constant. As always, $T < 1$. Thus, the Lambert approach always yields $\alpha d > 0$ in the region with no absorption.

Moss *et al.* [2] presented a method to derive a formula to account for the interference effects in a thin film. Excluding the effects induced by the rear face of the material and averaging the interference bands of a spectrum [2], the approximate transmissivity will be

$$T = (1 - R)^2 e^{-\alpha d}\,. \tag{12}$$

Then,

$$\alpha d = \ln\left[(1 - R)^2/T\right]\,. \tag{13}$$

Here, T is the measured transmittance from the first side of the film into a substrate and R the reflectance of the film material,

$$R = \frac{(n-1)^2 + k^2}{(n+1)^2 + k^2}\,. \tag{14}$$

In practice, R is typically taken as a measured reflectance of a sample together with its back surface. In this case, if the reflection is measured on the film side of the sample, the real measured reflectance (presented using the definitions from (14)) for a system film-substrate is

$$\mathcal{R} = R + \frac{T^2 r}{1 - Rr} = R + \frac{T^2 (n_0 - 1)^2}{(n_0 - 1)^2 - R(n_0 - 1)^2} \tag{15}$$

and the real measured transmittance

$$\mathcal{T} = \frac{Tt}{1 - Rr} = \frac{4nT}{(n_0 + 1)^2 - R(n_0 - 1)^2} \,. \tag{16}$$

Here t and r denote the transmittance and reflectance of the semi-infinite rear surface of a sample (Figure 1). If a substrate rear surface is in contact with air,

$$t = 4n_0/(n_0 + 1)^2 \tag{17}$$

and

$$r = \frac{(n_0 - 1)^2}{(n_0 + 1)^2} \,, \tag{18}$$

where n_0 is the refractive index of the non-absorbing substrate. In this case, we always have $R < 1; T < 1$ for substrates with low refractive index $(n_0 - 1)^2 \ll (n_0 + 1)^2$. Therefore

$$\mathcal{T} \simeq 4n_0 T/(n_0 + 1)^2 \,, \tag{19}$$

$$\mathcal{R} \simeq R + \frac{T^2 (n_0 - 1)^2}{(n_0 + 1)^2} \simeq R \,. \tag{20}$$

This approximation yields the absorption coefficient

$$\ln\left[\frac{(1 - \mathcal{R})^2}{\mathcal{T}}\right] = \alpha d = \ln\left[\frac{(1 - \mathcal{R})^2 (n_0 + 1)^2}{4n_0 T}\right] \,, \tag{21}$$

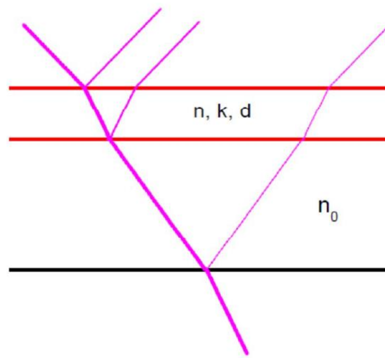

Figure 1. Sketch of the thin absorbing film on a transparent substrate.

and, as in the region of low absorption near the absorption edge, $1 - \mathcal{R} \approx \mathcal{T}$, there should always be

$$\alpha d = \ln\left[\frac{(n_0+1)^2\mathcal{T}^2}{4n_0 T}\right] = \ln\left[\frac{\mathcal{T}^2}{Tt}\right] < 0\,, \tag{22}$$

as $\mathcal{T} < T \leq t$.

In the approximation by W.Q. Hong [3] for substrates with low refractive indices in the range of $1.5 < n < 1.7$, the reflections from the rear faces of the films and the substrates were also excluded, considering that they only marginally influence the reflectance.

In this case, the obtained result was

$$\alpha d = \ln\left[\frac{(1-\mathcal{R})}{\mathcal{T}}\right]\,, \tag{23}$$

and in the low absorption region

$$\alpha d = \ln\left[\frac{\mathcal{T}}{\mathcal{T}}\right] \simeq 0\,, \tag{24}$$

as $1 - \mathcal{R} \approx \mathcal{T}$.

One more approach may be based on the formula

$$T = \frac{(1-R)^2 e^{-\alpha d}}{1 - R^2 e^{-2\alpha d}}\,, \tag{25}$$

which is applicable for a slab of absorbing material [1, p.93]. Here, T is the full transmittance of a slab, R is the reflectance of one side of the material and the effect of the substrate is neglected. Solving the equation, we get

$$e^{-\alpha d} = -\frac{1}{2TR^2}\left[(1-R)^2 \pm \sqrt{(1-R)^4 + 4T^2R^2}\right]\,. \tag{26}$$

If the slowly changing member R^2 is dropped from the equation, the result will be an absorption coefficient

$$\alpha = \frac{1}{d}\ln\left[\frac{(1-R)^2}{2T} + \sqrt{R^2 + \frac{(1-R)^4}{4T^2}}\right]\,. \tag{27}$$

The formula above has been used in [4–6]. Again, instead of R, the full reflectance of the sample was used. The outcome is approximately the Moss formula with one additional member.

Using spectrometric ellipsometry (SE), the measured film spectra can be modeled according to a pre-set dispersion formula to obtain film thickness and its dispersion values parametrically. The simplest of the used dispersion relations

for this purpose is the Cauchy formula, either in Cauchy approach with absorption index defined as a step function

$$n(\lambda) = A + \frac{B}{\lambda^2} + \frac{C}{\lambda^4}\,, \qquad k(\lambda) = D + \frac{E}{\lambda^2} + \frac{F}{\lambda^4}\,, \tag{28}$$

or in Cauchy-Urbach approach, where refractive index dispersion is presented in Cauchy form and absorption as the Urbach tail

$$k(\lambda) = \alpha \exp\left[\beta\left(\frac{1}{\lambda} - \frac{1}{\gamma}\right)\right]. \tag{29}$$

Subsequently, the absorption edge can be determined based on the obtained values. The more elaborate dispersion relations are also used, including ones where the absorption edge value is a parameter of the model (Sellmeier, Tauc-Lorentz). However, neither of them employs the absorption coefficient dependency as a parabolic or square root against the energy as it is proposed in the absorption edge modelling based on the parabolic bands. One more possibility is performing reverse calculation on the measured data, if it is possible, to get a more realistic dispersion dependency for later use.

To identify the most popular methods to detect the absorption edge, we conducted a literature review based on the papers dealing with ZnO band gap and presented by Viezbicke *et al.* [7]. Table 1 presents the different methods employed to detect the absorption edge along with the formulas that were used. Most of the papers analyzed in the literature review were quoted in [7], the others were those found by us concerning the band gap of ZnO. Of the papers from [7], 32 are not quoted here as they have not indicated a method used to calculate absorption. The formulas in Table 1 are given as they were presented by the authors of the papers, some probably not in a form they were really used.

Of the presented methods, the spectrophotometric calculations do not depend on any dispersion model. The methods based on ellipsometric modelling are mostly not consistent with Kramers-Kronig relation, but useful for use in limited spectral region. Tauc-Lorentz and Forouhi-Bloomer dispersions fulfill the Kramers-Kronig relation also.

According to Table 1, the most used formula for calculating the absorption coefficient is based on the Lambert absorption model where the effects of interference in the film are ignored. Occasionally, methods like the Kubelka-Munk approach, which is based on the analysis of diffuse reflectance spectra with the scattering effects playing a major part, or different derivative methods, or SE with different dispersion formulas are used (Table 1). The Kubelka-Munk approach is mainly applied for the films or materials comprising clearly defined particles where the absorption coefficient α is substituted for the equivalent absorption units

$$F(R) = (1-R)^2/(2R) \tag{30}$$

[103, 104]. In the case of the derivative methods, different dependencies

Table 1. Use of the different methods to calculate the absorption coefficient for ZnO

Method	Formula	Quoted by Viezbicke [7]	Other works
Beer-Lambert	$\alpha d = \ln(1/T)$	[8–32]	[33–67]
Beer-Lambert with accounting for the substrate reflections	$\alpha d = \ln(T_0/T)$	[68–71]	[72]
	$\alpha d = \ln(T)$		[73]
Hong [3]	$\alpha d = \ln\left((1-R)/T\right)$		[74–83]
	$\alpha d = \ln\left(T/(1-R)\right)$	[84]	[85]
Moss [2]	$\alpha d = \ln\left[(1-R)^2/T\right]$		[86–92]
	$\alpha d = \ln\left[(1-R)^2/(2T)\right]$	[15, 19, 93]	
	$\alpha d = \ln\left[T/(1-R)^2)\right]$		[94]
Variants of Salem [5]	$\alpha d = \ln\left(\frac{(1-R)^2}{2T} + \sqrt{R^2 + \frac{(1-R)^4}{4T^2}}\right)$	[95]	[50, 96]
	$\alpha d = \ln\left[\frac{1}{R^2}\left(-\frac{(1-R)^2}{2T} + \sqrt{\frac{(1-R)^4}{4T^2} + \frac{R^2}{4}}\right)\right]$		[97–99]
Envelopes [100, 101]			[66, 102]
Kubelka-Munk [103]	$F(R) = \frac{(1-R)^2}{2R}$	[104]	[105–107]
	$\alpha = \frac{2.303A\rho}{IC}$	[108]	
Iterative methods		[10, 109]	
Derivative methods		[14, 26]	[96, 105] [110–113]
Diffuse reflectance		[114]	
Cauchy-Urbach		[115]	
Urbach tail	$\alpha = \alpha_0 \exp\left(\frac{h\nu}{E_0}\right)$	[116]	[96]
SE, Cauchy dispersion		[117]	
SE, Cauchy-Urbach		[118]	[58, 119]
SE, Sellmeier dispersion			[120]
SE, Tauc-Lorentz dispersion			[121–123]
SE, Forouhi-Bloomer dispersion			[124, 125]
SE, multi-parameter			[123] [126, 127]

($dT/d\lambda$, dT/dE or $d\alpha/dE$) are used and the absorption edge is defined as the position of the obtained maximum.

Additionally, the absorption term to characterize the absorption can be defined by different conventions. Typically, the variable used in absorption calculations is $\alpha\hbar\omega$ [6,8–13,16,19–21,38–40,46,48,49,56,58,68–70,72,73,80,83,84,93,94, 109,123]. This approach is based on the study by Tauc [128] where, in reality, a variable $\sqrt{\varepsilon_2}\omega = \omega\sqrt{2nk} = \omega\sqrt{n\alpha c} \sim \sqrt{\alpha n E}$ [129], if

$$\alpha = 4\pi k/\lambda = 4\pi k\nu/c = 2k\omega/c \tag{31}$$

is considered, was used. Some sources use other variables such as α [9,27,122, 130], and $\alpha h\nu n$ [131]. Khoshman et al. [119] used both the parameters $\alpha\hbar\omega$ and $\alpha\hbar\omega n$ in their study.

Conversely, a-Si:H type materials were shown to produce the better results [132, 133] when the dipole matrix element was used to derive a dispersion function, instead of the Tauc approach using the momentum matrix element. In this case, we get the variable $\sqrt{\alpha n/E}$. Even different formulas are obtained using a semi-classical approach [134].

We can suppose that the different calculation methods lead us to the different numerical values. To understand how the different models work in case of thin films, we performed an analysis of some theoretical thin films and the $Hf_xTi_yO_z$ films deposited using the atomic layer deposition (ALD) method with different approaches.

Formerly, for ALD-grown HfO_2 films, the absorption edge has been reported at a region of 5.55-5.8 eV [135], for sputtered TiO_2 at 3.0 or 3.2 eV [136] and for epitaxial TiO_2 films at 3.37 and 3.51 eV [137]. A previous study of the TiO_2 films mixed with the oxides of Hf, Ta or Sr demonstrated that all the analyzed films possess the indirect type of transition characteristic for TiO_2 [131, 136]. For mixed materials $Ta_2Ti_3O_z$ and $Sr_xTi_yO_z$ only TiO_2-type bandgaps were seen for optical measurements, although the bandgaps for both oxides were marked in photoconductivity measurements. Meanwhile, for $Hf_xTi_yO_z$ films the Hf atoms prevent a full overlap of the d-states for neighboring Ti-cations, resulting in a change of the absorption edge position dependent on Hf concentration [131].

2 Experimental Method

We analyzed the ALD coated hafnia-titania films as the different absorption edges could be seen at changing the relative composition of a mix of the same materials [131]. The $Hf_xTi_yO_z$ films were deposited on SiO_2 and Si(100) substrates in a low-pressure flow-type ALD reactor [138]. Both used hafnium-titanium oxide films were deposited using supercycles. In first case (Film A), the each of the supercycles contained 1 cycle for deposition of HfO_2 followed by 2 cycles for deposition of TiO_2 and the supercycle was repeated 500 times.

In the second case (Film B) 1 cycle for deposition of HfO_2 was followed by 5 cycles for deposition of TiO_2 and it was repeated 250 times. Both films were grown at a substrate temperature of 350°C. The detailed deposition parameters have been described in a previous study [139].

The composition of the material was analyzed on Si(100) parallel object using an X-ray fluorescence (XRF) analyzer ZSX400 (Rigaku) and the results are presented in Table 2. The phase composition was characterized by the grazing incidence X-ray diffraction (GIXRD) method using an X-ray diffractometer SmartLab (Rigaku). Both measured samples were amorphous.

Table 2. Chemical composition of the deposited mixed oxide films

Sample	Hf mass thickness, $\mu g/cm^2$	Ti, $\mu g/cm^2$	Cl, $\mu g/cm^2$	Atomic relation, Hf/(Hf+Ti)
A	455	101	0.016	0.55
B	255	118	0.012	0.37

The transmission and reflection spectra of our films grown on fused silica were recorded on a spectrophotometer "Jasco V-570". The spectral resolution at measurements was 1 nm, the measurement accuracy 0.5%. The results were corrected against the 100% line registered with empty measurement chamber for transmission and against a reference Al mirror for reflection. Subsequently, reflectance values of the reference mirror were calibrated against the values obtained from a good quality fused silica sample using experimental values of the SiO_2 refractive index [140] and the measured reflection values corrected accordingly.

The ellipsometric measurements of the transmissive samples were performed on a spectroscopic ellipsometer GES-5E from "Semilab Co." using a microspot mode to avoid interference from the rear face of the substrate, incidence angle of a beam at measurement was 70°. A SEA program was used to analyze the obtained spectra according to Tauc-Lorentz and Cauchy-Urbach dispersion formulae. Additionally, a reverse calculation of the dispersion was performed using WinElli-II program resulting in the numeric values of the complex refractive index over the spectrum. For this purpose, the film thickness values from Tauc-Lorentz model were used with a marginal variation of a film thickness when needed.

3 Modelling

To demonstrate how the different models work in case of the thin films, we calculated the transmission and the reflection spectra of a theoretical 202 nm thick film to obtain the enhanced influence of the dispersion and interference effects on the film absorption. In those calculations the refractive index of the

substrate, if not stated otherwise, was taken as $n_0 = 1.5 + 0.01E^2$ and that of a film, $n = 2+0.02E^2+0.001E^4$ with energy E presented in electron-volts. Film absorption in classical approach was initially defined as $k = 3\sqrt{E-2}/(2E)$ in the case of direct absorption and $k = 3(E-2)^2/(2E)$ in the case of indirect absorption. In both types of absorption, the onset of absorption occurred at 2 eV, after which absorption rose to a value of $k = 0.5$ at 3 eV energy. This effect is the consequence of a selected dependency of absorption on energy

$$\alpha\frac{4\pi k}{\lambda} = \frac{4\pi kE}{hc} \sim (E-E_0)^n \tag{32}$$

with n equal to $1/2$ for direct or 2 for indirect transitions. The interference effects in thin films were considered while the rear surface of the substrate was taken to contribute noncoherently in the calculations. The given dispersion model is shown in Figure 2. The calculated transmission and reflection spectra for these situations are presented in Figures 3a,b.

From the obtained dispersion, we can calculate the absorption parameters using different absorption models. The spectra of the absorbance αd results in these approximations for both types of absorption are presented in Figures 4a,b.

As shown previously, the Moss and Salem approaches result in negative absorbance and the Lambert approach results in positive absorbance in the transmission region. In contrast, the Kubelka-Munk approach presents clearly different dependencies owing to the fact that it is meant for scattering media where the calculated absorption is affected not by interference but by the multiple scattering processes. Therefore, we excluded this approach from our farther study. The results for the Hong model coincide with the values obtained from direct calculation of the films using the absorption index, k, and its dependence on

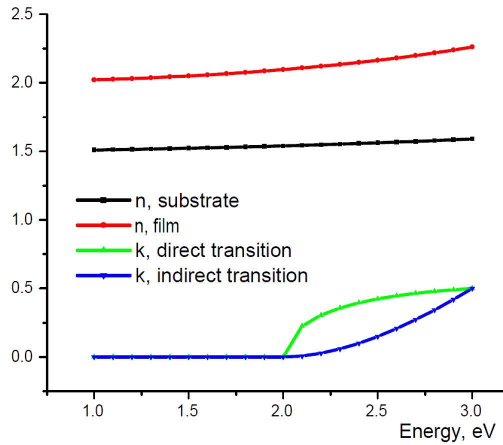

Figure 2. Used dispersion model for calculating the reflection and transmission spectra.

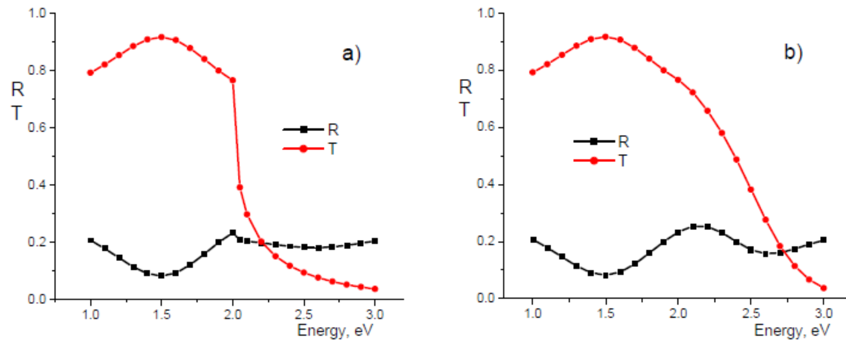

Figure 3. Reflection and transmission spectra for absorbing thin film on a non-absorbing substrate: (a) direct; and (b) indirect transition.

energy.

If the results are presented in the square and square root scales, the most precise outcome is again achieved with Hong formula, whereas the Moss and Salem approaches (in the case of direct transitions coinciding on this graph) result in higher absorption values, and the Lambert approach results in lower absorption edge values (Figure 5a). In the case of indirect transition, the situation is more complicated as an additional structure is created in the spectra. This additional structure arises because an absolute value of the optical density must be taken before calculating the root function in the near zero and zero absorption region for Moss and Salem approaches. Fortunately, this undesirable addition can be avoided by removing the part of spectrum near the zero absorption and extending a line to zero. However, despite this procedure, the absorption edge value obtained would still be on the higher energy side (Figure 5b). In this case, a zero

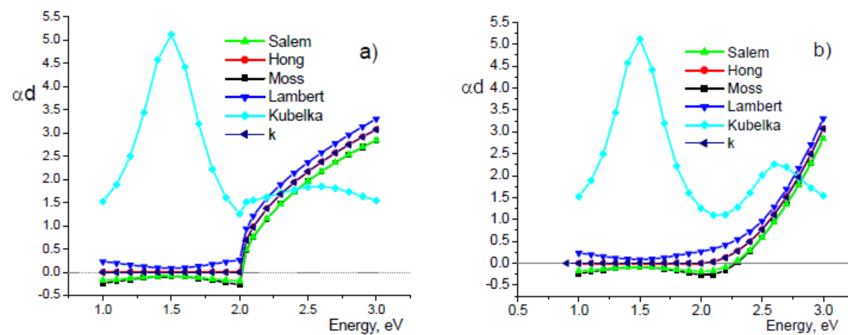

Figure 4. Calculated absorbance spectra for absorbing thin film using different approximations: (a) direct; and (b) indirect transition. The Hong approach is covered by film model values (k); the Moss and Salem approaches yield almost equal results.

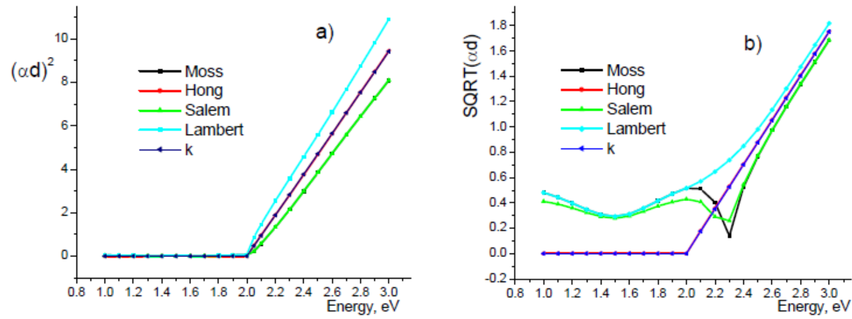

Figure 5. Reverse calculation of absorption edge in: (a) direct; and (b) indirect case. The Hong approach is covered by film model values; Moss and Salem approximations are indiscernible for direct transition.

absorption value is obtained at the point where the calculated absorbance graph moves from the positive to the negative side of the absorption values, not in a real minimum.

Furthermore, in the case of direct transitions, the square function part of the calculated optical density spectrum far from zero point is amplified and the negative effects in the transmission region are less visible. In the case of a root function, the opposite occurs – the values of high absorption diminish and the structural effects of the calculation become more evident.

The impact of the edge effects caused by the transmissive region of the spectrum can be corrected by taking two points in the spectrum at the transmission region where absorption should be absent, and defining the optical density at those

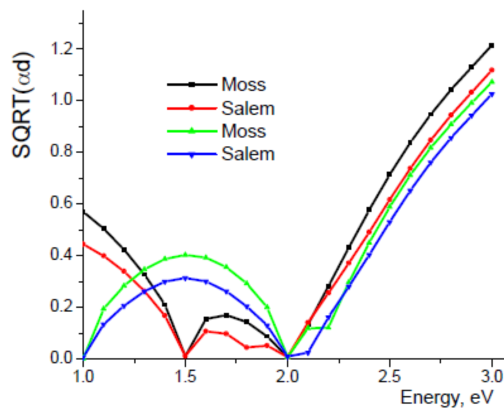

Figure 6. Correction of the absorption in indirect case. The absorption is defined being zero either at 1.0 and 2.0 eV or at 1.5 and 2.0 eV.

points as zero [141]. Subsequently, the linear dependence of the absorption energy between these points can be determined and the calculated spectrum in a region near the absorption edge can be transformed so that our predefined points move to a zero line. If the predefined points are near the absorption edge, this part of the calculated optical density should also move closer to zero. The result will improve our situation, but unfortunately will still be dependent on a choose of our base points as shown in Figure 6 where the correction procedure has been implemented using two different choices. For Lambert approach the correction was less effective compared to Moss or Salem approaches in case of the direct transition and in case of indirect transition (not shown) it was not feasible at all. This happens due to the positive values for the absorption coefficient over the entire spectral region making it problematic to find the zero-absorption energy values for the correction process.

As the interference effects are a function of an optical thickness of the analyzed film, it is worth to look how the results depend on it. According to the calculation for the dispersion used in this work film thicknesses 296 and 370 nm are corresponding to full-wave and 5λ/4 optical thickness at 2 eV, respectively. The calculation results for these cases are presented on Figures 7a,b for two types of transitions. From here up to Figure 12, the model absorption values are not presented more as the purpose is to compare the behavior of the different calculation approaches. Salem dispersion model is left out from now as its results coincide with those for Moss model for thicker films with direct transition and differ only a bit in case of indirect transition. There is a slope increase with film thickness for both cases indicating movement to more precise results (they are less dependent on dispersion effects). The calculation results for Moss and Lambert approaches in transmission region coincide (Fig. 7b) due the models presented as $\alpha d = \ln\left[(1-R)^2/T\right]$ for Moss approach and $\alpha d = \ln(1/T)$ for Lambert approach. In the transmission region there is

$$1 - R = T\,, \tag{33}$$

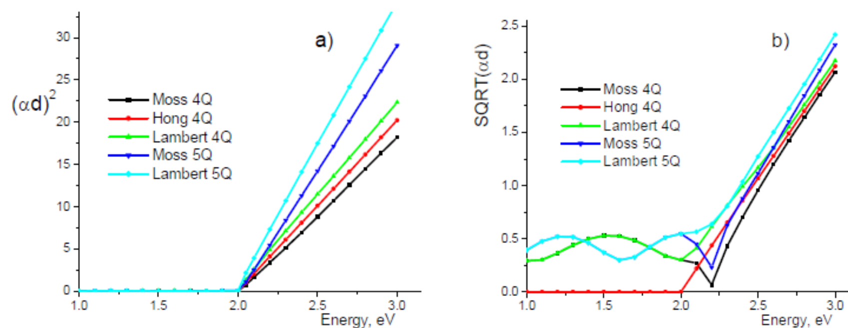

Figure 7. Direct (a) and indirect (b) transitions for films with different thicknesses (in optical quarterwaves) using the different approaches.

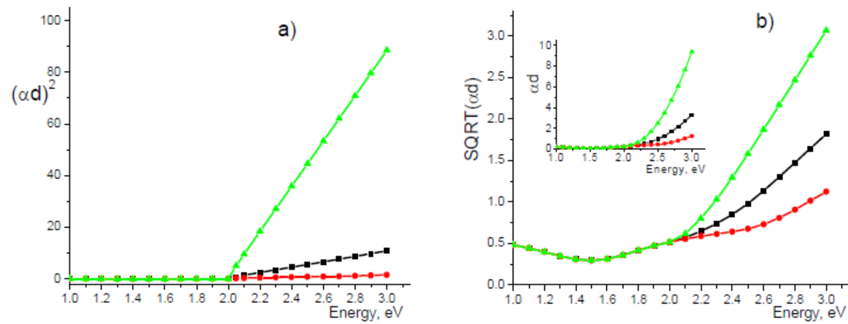

Figure 8. Absorption edge for Lambert absorption. Direct (a) and indirect (b) transitions for 202 nm thickness film and different absorption levels (see text). Inset for indirect transition presents the optical density.

therefore,

$$\alpha d = \ln\left[T^2/T\right] = \ln(T) = -\ln(1/T)\,. \qquad (34)$$

After using a square (direct transition) or absolute function (indirect case) the different signs are eliminated and the results will be the same. The results of the Lambert model for indirect transition are more problematic for analysis as the calculation results turn away from zero line near the real onset of the absorption. In Figures 8a,b, there are the reverse calculation results for the Lambert model having different levels of the absorption – the films have a same refractive index dispersion but the absorption index dependencies are peaking at 0.167, 0.5 and 1.5 level at 3 eV. For high absorption levels and direct transition model, the result is appropriate. However, for lower absorption levels, the decent results can be obtained only using linear correction (Figure 9). The low absorption

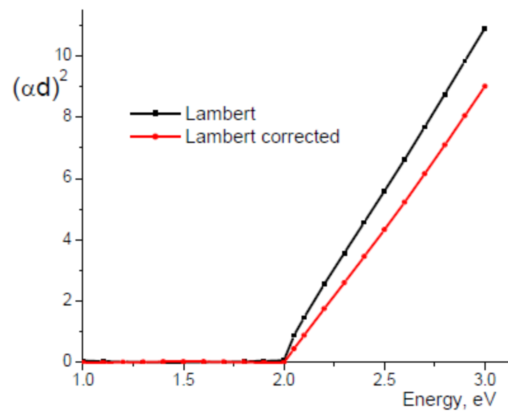

Figure 9. Correction of Lambert absorption for direct transition, 202 nm film with $k = 0.5$ at 3 eV.

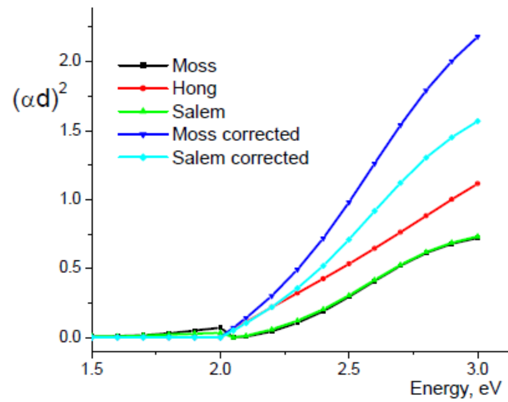

Figure 10. Correction of the absorption results for direct transition, $k = 0.167$ at 3 eV, correction points 1.5 and 2.0 eV. Without correction, the correct result for absorption edge using Moss or Salem models is unattainable. Moss and Salem absorptions before correction almost coincide.

levels create problems in constructing a linear dependence and finding its point of contact with the zero line for the other approaches also (Figure 10). Therefore, for thin films with lower absorption levels, situations may exist where the results are unobtainable at all in the case of indirect transition (Figure 8b).

We see that the most accurate method to determine the absorption edge for thin films is the Hong approach, which gives us the linear dependencies as expected. Its region of use is even greater than that claimed by Hong [3] as can be seen for the substrates with lower and higher refractive indices (Figure 11ab). For even thinner films (not shown) the same structural differences between the different

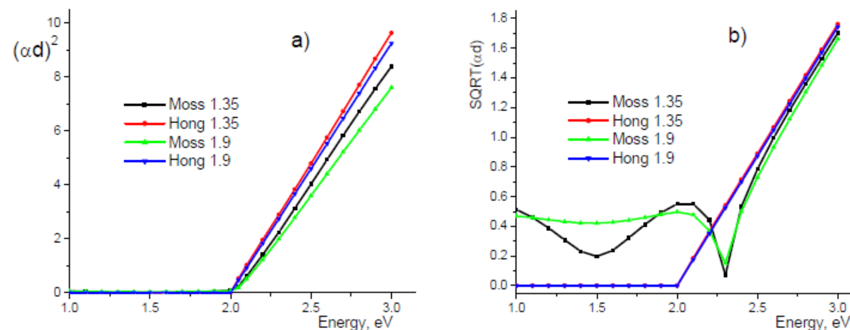

Figure 11. Hong and Moss absorption results for substrates with different refractive indices for: (a) direct; and (b) indirect cases. 1.35 – refractive index of a substrate in the range of 1.31–1.39 in the 1–3 eV region, 1.9 – refractive index of a substrate being in the range of 1.82–1.98. Moss absorption results are not corrected.

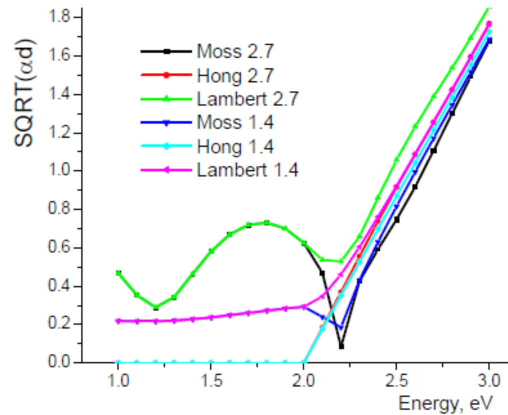

Figure 12. Moss, Hong and Lambert absorption results for films with indirect transition having a refractive index dispersion from 2.53 to 2.85 (2.7) or from 1.31 to 1.47 (1.4) in the presented region.

approaches continue to exist. However, in the cases of thinner films, we need to deal with higher measurement uncertainties also.

Additionally, as shown in Figure 12 for the case of two films with the same thickness (202 nm) and absorption index (reaching 0.5 at 3 eV) but different refractive index dispersions (i.e. 2.53–2.85 and 1.31–1.47), the results are clearly dependent on the refractive index of the film. This effect is weaker in films with low refractive indices, whereas for films with high refractive indices, the influence of the interference effects can be observed even in the absorption region. Contrary, the graphs for the two films with different refractive indices obtained using the Hong approach are not discernible.

As previously mentioned, the results of the calculations may differ dependent on the variables used. Nevertheless, in our case, where the used energy region was from 1 to 3 eV, including the energies in the calculations would result in energy values that differed from each other by a factor of 3, for direct transition absorbance dependencies by a factor of 9 (square function) and for indirect transition by a factor of 1.7. This discrepancy in values would clearly influence the results obtained using Moss and Lambert approaches in case of the indirect transition but would have only a minor effect on those obtained using the Hong and direct transition Moss approaches (Figures 5ab).

4 Experimental Results

To demonstrate how the different models can be used to calculate the absorption edge and to present the possible problems that can occur, we analyzed two $Hf_xTi_yO_z$ films. Films with different chemical compositions of Hf and Ti were

deliberately selected to highlight possible problems (Table 2). The thicknesses of Films A and B according to the analysis using Tauc-Lorentz dispersion model were 93.5 and 75.5 nm, respectively. GIXRD demonstrated that both films were amorphous (not shown). Based on the existing knowledge we will deal mainly with indirect absorption edge, if not stated otherwise.

The absorption coefficients of the films were calculated from the transmission and reflection data using the Lambert, Hong, Moss, and corrected Moss methods; from the SE spectra using Tauc-Lorentz and Cauchy-Urbach dispersion models; and with a reverse calculation of the optical constants using WinElli-II program, the film thicknesses taken there as obtained from Tauc-Lorentz dispersion model (Figures 13a and b).

To obtain the corrected Moss absorption dependence, the results were set to zero in the case of film A at 1.5 and 3.7 eV and in the case of film B at 2.3 and 3.7 eV, and the spectra were linearly transformed. For both films the Tauc-Lorentz modelling was performed up to 5 eV. Whereas, the Cauchy-Urbach dispersion model could be used only up to 4.5 eV in the case of film A. In the case of film B Cauchy-Urbach dispersion did not give a correct fit to the measured SE spectra. This dissimilar range of usage of the two models in case of film A can be attributed to the differences in character, as the Tauc-Lorentz dispersion enables us to reach further into the high absorption levels in the conductivity band.

Figure 13 shows that most of the methods present relatively similar absorption coefficient dependencies. The main differences are shown in case of film A in the tail in the UV region using the Lambert approach and the negative absorption values for Moss approach. In the case of film B, the Lambert approach yields clearly lower absorption values in the high absorption region. In both cases the reverse calculation fails in the visible transmissive region and highly absorptive regions over 3.9 and 4.2 eV in case of samples A and B, respectively.

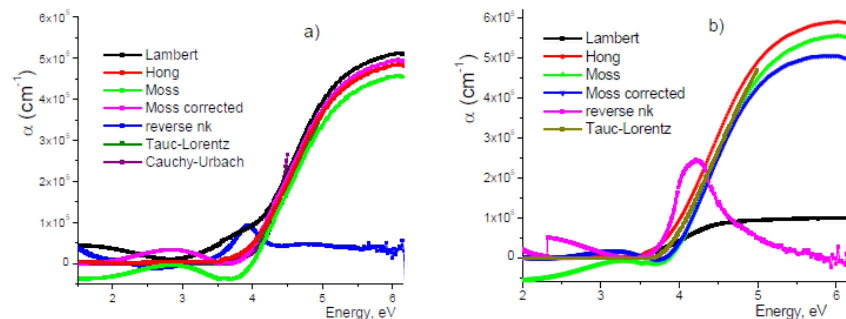

Figure 13. Absorption coefficient dependencies of: (a) Film A; and (b) B using different calculation methods. In case of Film A the Tauc-Lorentz result is almost covered by corrected Moss and Hong curves.

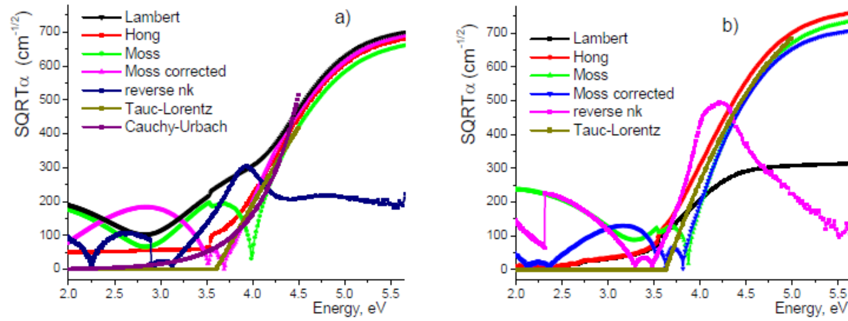

Figure 14. Absorption edge of: (a) Film A; and (b) B using the indirect approach.

The square roots of the absorption coefficient obtained using the different models are represented in Figures. 14a and b. The absorption edge values obtained from the slope of the function are between 3.4 (Lambert) and 4.0 eV (Cauchy-Urbach and Moss) and 3.2 eV (Lambert) and 3.9 eV (Moss) for films A and B, respectively (Table 3). Compared to the other methods, remarkably lower values are obtained with the reverse calculation for film A at 3.1 eV. Meanwhile, the values obtained using the Moss approach for both films are the highest. The Hong approach results in a relatively linear dependence for film B, giving an absorption edge value of 3.5 eV if a line is drawn from 3.6 to 4.1 eV. However, in this case a long absorption tail exists in the visible region, which could be the Urbach tail.

Furthermore, the TRA method (Figure 15, Table 3) can be used if the transmission and reflection values are correctly measured. In this method, the absorption

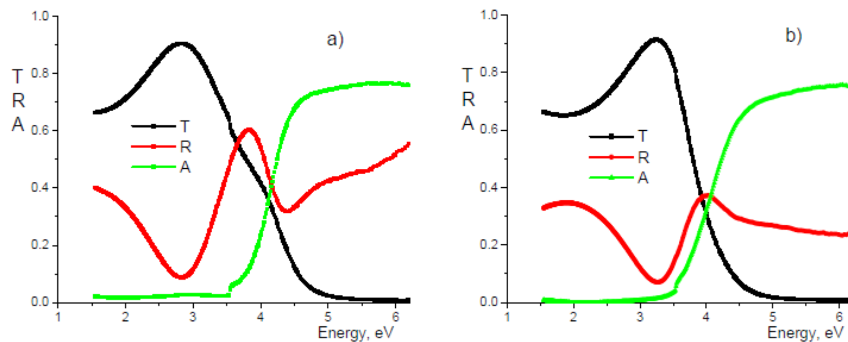

Figure 15. Transmission, reflection and absorption results for: (a) Film A; and (b) B. The absorption values for the entire film were obtained as $A = 1 - T - R$ after correction of the transmission results against empty chamber transmission results and the reflection values against reference Al mirror reflection at first and against pure SiO_2 sample reflection spectrum afterwards.

Table 3. The absorption edge values for films A and B obtained by different methods using the indirect transition approach (eV). For the Hong method, a result for the direct transition approach has been added for comparison

Method	Film	
	A	B
Lambert	3.4	3.2
Hong	**3.7** (3.6)	**3.4** (3.6)
Moss	4.0	3.9
Moss corrected	3.7	3.8
Reverse ellipsometry	3.1	3.5
Tauc-Lorentz	3.6	3.6
Cauchy-Urbach	3.5–4.0	
Lambert and Moss	3.5	3.7
T R A	3.5–3.8	3.5
Direct transition Hong	4.3	4.2

edge can be evaluated directly from the spectrophotometric spectra. Another method to determine the absorption edge position is to find the coincidence point of the Moss and Lambert approaches, as explained in Section 3. In the case of the indirect approach, the coincidence points are at 3.5 and 3.7 eV for films A and B, respectively.

For film A, different edge values can be obtained using the Cauchy-Urbach model, depending on the region of evaluation. The same situation can be encountered for spectrophotometric values where the measurement peculiarity is situated near the location of the edge. In the case of the Hong approach for film A, the first result is preferable when a straight line is drawn to the plateau, and not to the mathematical zero line. For film B, the Hong approach value depends on whether it is defined at the zero absorption point on the axis or at the point where the Urbach tail gives ground to the fundamental absorption.

A nonzero absorption in the visible region and a “bump” seen between 3.6 and 3.8 eV for the Hong approach can be attributed to the measurement flaws of a spectrophotometer (Figure 14a). In the latter case, lower transmission values can be seen (Figure 15a) in the higher energy region after the grating change of a spectrophotometer at 350 nm (3.55 eV). Conversely, this effect could be induced by the manifestation of the Urbach tail in the film.

The Urbach tail that manifests itself owing to delocalized states in the band gap or structural imperfections is defined as

$$\alpha(E) = \alpha_0 \exp\left(\frac{\sigma(E - E_0)}{kT}\right) . \tag{35}$$

If we drop the temperature dependence from the equation, we get

$$\alpha(E) = \alpha_1 \exp\left[A(E - E_0)\right] . \tag{36}$$

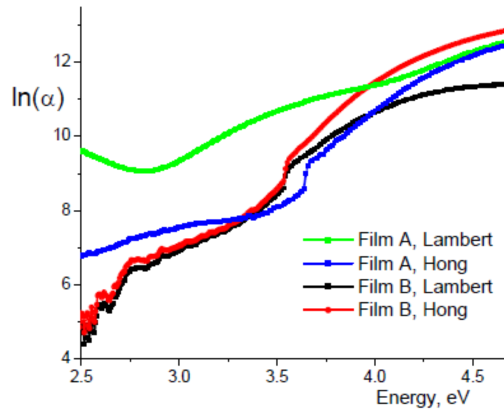

Figure 16. A modelling of possible Urbach tail for our films.

Therefore,

$$\ln(\alpha) = \ln(\alpha_1) + [A(E - E_0)] = AE + [\ln(\alpha_1) - AE_0] \ . \qquad (37)$$

To qualify as the Urbach tail, the logarithm of the absorption coefficient must be a linear function of energy. To check whether our films met this requirement, a logarithm of their absorption coefficients is shown in Figure 16. For film A, the region of interest lies between 3.5 and 3.8 eV; for film B, between 2.4 and 3.5 eV (Figure 15ab). The results show that this treatment can be applied to both films (for film B from 2.8 eV onwards) in case of the Lambert and Hong approaches. However, considering the presence of a clear drop near the point of grating change of the spectrophotometer, the possibility of measurement flaws cannot be excluded. As the purpose of this study is to assess the effectiveness of the different models used to calculate the absorption coefficient, this problem is set aside for the moment, and will be taken up in future studies.

Figure 17 presents the absorbance values for our model dispersion used in Section 3. The reflectance values used in the calculations are shifted either at 2% lower (- case) or at 2% higher (+ case). In both cases, the calculated absorption values rise for lower reflectance (because energy loss is considered as absorption in the calculations) and fall for higher reflectance. For the Hong approach, the absorption coefficient values remain flat and the experimentally determined differences can be easily compensated. Therefore, our defined point of absorption onset may be found as not a point of coincidence of calculated line with a computed zero absorption value, but a coincidence with a height of the plateau in the visible region. However, the results obtained with Lambert and Moss approaches remain dependent on film thickness (Figure 7b). Therefore, such automatic correction cannot be used for these models.

The SE calculations, strictly speaking, must result in neither direct nor indirect

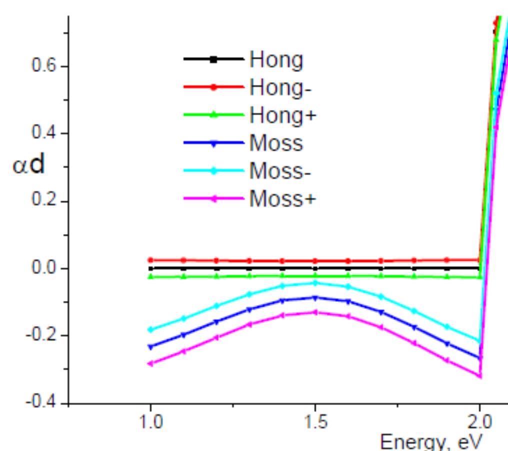

Figure 17. The changes in the calculated absorption coefficient for Hong and Moss models if the errors in reflection measurements are introduced.

transition linear dependencies because the dispersion formulae used for characterizing absorption do not contain this type of term. However, Lee *et al.* [142] demonstrated in their study that the SE Tauc-Lorentz, Forouhi-Bloomer and the modifications of Forouhi-Bloomer dispersion formulae enable us to find a suitable linear region of the results, to ensure that we obtain at least a numerical value for the absorption edge.

In the case of thin films, both direct and indirect transition models can possibly present a linear dependency [62, 143, 144]. However, as the processes inducing these types of behavior are different, a transition cannot be direct and indirect simultaneously. Figure 18 represents the results for direct transition edge calculations for film B. According to all the Hong, Moss, and Tauc-Lorentz approaches, the absorption edge value in case of direct transition would be 4.2 eV, if calculated from the energy region between 4.3 and 4.7 eV. The results of spectrophotometry clearly demonstrate that no connection is seen between the absorption edge value deduced from direct transition model and that obtained from the real absorption of this film (Figure 15b). However, the simultaneous edges for two different transitions may be registered if both types of transitions exist near the absorption edge as shown in certain previous studies [6, 145, 146].

This lack of coherence between the spectrophotometric data and the direct transition model clearly indicates that the absorption edge of our material has an indirect character. The various methods to determine the absorption edge position give us results that deviate up to 10% on either side when compared with the Hong approach. Therefore, it is important to specify the calculation method used to find the absorption coefficient. Interestingly, the simplest and most popular, as shown in Table I, Beer-Lambert method yields the lowest values for absorption edge position.

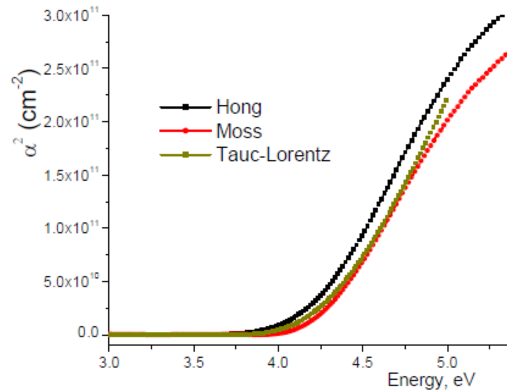

Figure 18. Absorption edge of Film B according to the direct transition model.

5 Conclusions

Our results show that a method chosen to calculate the material absorption coefficient values has the profound influence on the obtained absorption edge (the energy for which the absorption coefficient α or the absorbance αd equals zero) value if the film thickness is below 1 μm. This can be attributed to the interplay of the absorption and interference effects. However, the change of the optical constant values over a large spectral region used for absorption coefficient calculation may also influence the measurement results. For the analyzed $Hf_xTi_yO_z$ films the different calculation methods yield the scatter of the absorption edge values within a range of about 0.6 eV. Among these, the Moss and Salem approaches persistently yield higher energy values for the absorption edge, whereas the Lambert approach yields the lowest values.

Furthermore, the results obtained depend on the absorbing material properties. More accurate results are obtained for direct transition materials. This behavior can be attributed to a characteristic of modelling – taking a square function of the absorption values for direct transitions amplifies a part of the spectrum with higher absorption and steepens the function slope. Whereas, taking a square root function for indirect transitions amplifies a part of spectrum with lower absorption along with the contributions from the internal reflections of the substrate. These effects decrease in the case of films with higher absorption or higher thickness. This results in the higher absorption and the steeper function slopes giving us better accuracy in finding the absorption edge value.

A method has been proposed to lessen the effect of interference on the absorption edge calculations for thin films. If we are able to define the positions in a spectrum where real absorption values should be equal to zero, we may perform a linear transform of the absorption values so that a calculated absorption in these

points approaches this condition. Subsequently, the absorption coefficient values near the edge are recalculated. The resultant slope meets the horizontal axis at a position nearer to one where the real zero absorption should be achieved. However, this correction is effective only in the case of direct transitions and barely improves the situation for indirect transition case.

Thin film absorption edge values presented in literature need to be treated with caution when the method of absorption coefficient calculation is not clearly stated. The comparison is more accurate between the values obtained with the same absorption calculation method and less dependable if the different methods have been used.

The preferred method for determining the absorption edge for thin films with thickness below 1 μm is the Hong approach, where the absorbance is calculated as

$$\alpha d = \ln\left[\left(1-\mathcal{R}\right)/\mathcal{T}\right] . \tag{38}$$

Here, $\mathcal{R}$ and $\mathcal{T}$ are the full reflectance measured from the film side and the transmittance of a system substrate – thin film.

Acknowledgments

This work has been supported by "Center of Excellence" Program SLTKT16141T and the Estonian Research Council Grants PRG753 and PSG448.

References

[1] J.I. Pankove (1975) "*Optical Processes in Semiconductors*", Dover Publications, Inc., New York.

[2] T.S. Moss, G.J. Burrell, B. Ellis (1973), "*Semiconductor Opto-Electronics*", Butterworth and Co (Publishers) Ltd. pp. 15-19.

[3] W.Q. Hong (1989) *J. Phys. D: Appl. Phys.* **22** 1384.

[4] R. Vahalová, L. Tichý, M. Vlček, H. Tichá (2000) *Phys. Stat. Sol. (a)* **181** 199.

[5] A.M. Salem (2003) *J. Phys. D: Appl. Phys.* **36** 1030.

[6] Y.A. El-Gendy (2009) *J. Phys. D: Appl. Phys.* **42** 115408.

[7] B.D. Viezbicke, S. Patel, B.E. Davis, D.P. Birnie III (2015) *Phys. Stat. Sol. (b)* **252** 1700.

[8] Y. Natsume, H. Sakata (2000) *Thin Solid Films* **372** 30.

[9] Y. Natsume, H. Sakata (2001) *J. Mat. Sc.: Mater. Electron.* **12** 87.

[10] S. Bandyopadhyay, G.K. Paul, S.K. Sen (2002) *Sol. Energy Mater. Sol. Cells* **71** 103.

[11] S.T. Tan, B.J. Chen, X.W. Sun, W.J. Fan, H.S. Kwok, X.H. Zhang, S.J. Chua (2005) *J. Appl. Phys.* **98** 013505.

[12] S.T. Tan, B.J. Chen, X.W. Sun, M.B. Yu, X.H. Zhang, S.J. Chua (2005) *J. Electron. Mat.* **34** 1172.

[13] S.T. Tan, B.J. Chen, X.W. Sun, X. Hu, X.H. Zhang, S.J. Chua J. (2005) *Cryst. Growth* **281** 571.

[14] D. Ramírez, D. Silva, H. Gómez, G. Riveros, R.E. Marotti, E.A. Dalchiele (2007) *Sol. Energy Mater. Sol. Cells* **91** 1458.

[15] E. Şenadim Tüzemen, H. Kavak, R. Esen (2007) *Physica B* **390** 366.

[16] K.-C. Liu, Y.-H. Lu, Y.-H. Liao, B.-S. Huang (2008) *Jap. J. Appl. Phys.* **47** 3162.

[17] S. Mandal, R.K. Singha, A. Dhar, S.K. Ray (2008) *Mater. Res. Bull.* **43** 244.

[18] X.-H. Lu, D. Wang, G.-R. Li, C.-Y. Su, D.-B. Kuang, Y.-X. Tong (2009) *J. Phys. Chem. C* **113** 13574.

[19] E.Ş. Tüzemen, S. Eker, H. Kavak, R. Esen (2009) *Appl. Surf. Sci.* **255** 6195.

[20] M. Smirnov, C. Baban, G.I. Rusu (2010) *Appl. Surf. Sci.* **256** 2405

[21] K.V. Gurav, V.J. Fulari, U.M. Patil, C.D. Lokhande, O.-S. Joo (2010) *Appl. Surf. Sci.* **256** 2680.

[22] Y.-S. Ho, K.-Y. Lee (2010) *Thin Solid Films* **519** 1431.

[23] X. Ma, J. Zhang, J. Lu, Z. Ye (2010) *Appl. Surf. Sci.* **257** 1310.

[24] C.-Y. Tsay, K.-S. Fan, S.-H. Chen, C.-H. Tsai (2010) *J. Alloys Comp.* **495** 126.

[25] J. Chen, H. Deng, N. Li, Y. Tian, H. Ji (2011) *Mater. Lett.* **65** 716.

[26] C.D. Bojorge, V.R. Kent, E. Teliz, H.R. Cánepa, R. Henríquez, H. Gómez, R.E. Marotti, E.A. Dalchiele (2011) *Phys. Stat. Sol. (a)* **208**, 1662.

[27] Z.-N. Ng, K.-Y. Chan, T. Tohsophon (2012) *Appl. Surf. Sci.* **258** 9604.

[28] S.K. Panda, C. Jacob (2012) *Solid State Electron.* **73** 44.

[29] O. Tari, A. Aronne, M.L. Addonizio, S. Daliento, E. Fanelli, P. Pernice (2012) *Sol. Energy Mater. Sol. Cells* **105** 179.

[30] S. Yang, Y. Zhang (2013) *J. Magn. Magn. Mater.* **334** 52.

[31] B. Rajesh Kumar, T. Subba Rao (2013) *Appl. Surf. Sci.* **265** 169.

[32] K.K. Nagaraja, S. Pramodini, P. Poornesh, H.S. Nagaraja (2013) *J. Phys. D: Appl. Phys.* **46**, 055106.

[33] A.A. EL-Fadl, G.A. Mohamad, A.B. Abd El-Moiz, M. Rashad (2005) *Physica B* **366** 44.

[34] S. Ilican, M. Caglar, Y. Caglar (2007) *Mater. Sc.-Pol.* **25** 709.

[35] T. Ghosh, M. Dutta, S. Mridha, D. Basak (2009) *J. Electrochem. Soc.* **156** H285.

[36] M.H. Mamat, M.Z. Sahdan, Z. Khusaimi, A. Zain Ahmed, S. Abdullah, M. Rusop (2010) *Opt. Mater.* **32** 696.

[37] A. El Amrani, F. Hijazi, B. Lucas, J. Bouclé, M. Aldissi (2010) *Thin Solid Films* **518** 4582.

[38] D.K. Kim, H.B. Kim (2011) *J. Alloys Comp.* **509** 421.

[39] J.D. Pedersen, H.J. Esposito, K.S. Teh (2011) *Nanoscale Res. Lett.* **6** 568.

[40] S. Zandi, P. Kameli, H. Salamati, H. Ahmadvand, M. Hakimi (2011) *Physica B* **406** 3215.

[41] H. Abdullah, S. Selmani, M.N. Norazia, P.S. Menon, S. Shaari, C.F. Dee (2011) *Sains Malaysiana* **40** 245.

[42] H. Karaagac, E. Yengel, M. Saif Islam (2012) *J. Alloys Comp.* **521** 155.

[43] S. Benramache, B. Benhaoua (2012) *Superlatt. Microstruct.* **52** 807.

[44] L. Pholds, M.E. Samiji, N.R. Mlyuka, B.S. Richards, R.T. Kivaisi (2013) Presented at 28th European Photovoltaic Solar Energy Conference and Exhibition, p. 2311.

[45] G. Tang, H. Liu, W. Zhang (2013) *Adv. Mater. Sci. Eng.* **2013** 348601.

[46] G. Shanmuganathan, I.B. Shameem Banu, S. Krishnan, B. Ranganathan (2013) *J. Alloys Comp.* **562** 187.

[47] X. Zhou, Y. Zhang, W. Shi, T. Guo (2013) *J. Mater. Sci: Mater. Electron.* **24** 362.

[48] Z.-Y. Ye, H.-L. Lu, Y. Geng, Y.-Z. Gu, Z.-Y. Xie, Y. Zhang, Q.-Q. Sun, S.-J. Ding and D. W. Zhang (2013) *Nanoscale Res. Lett.* **8** 108.

[49] V. Kumar, N. Singh, R.M. Mehra, A. Kapoor, L.P. Purohit, H.C. Swart (2013) *Thin Solid Films* **539** 161.

[50] A.-S. Gadallah, M.M. Al-Nahass (2013) *Adv. Cond. Matter Phys.* **2013** 234546.

[51] A. Srivastava, N. Kumar, S. Khare (2014) *Opto-Electron. Rev.* **22** 68.

[52] A. Srivastava, N. Kumar, K.P. Misra, S. Khare (2014) *Mater. Sci. Semicond. Process.* **26** 259.

[53] A. Srivastava, N. Kumar, K.P. Misra, and S. Khare (2014) *Electron. Mater. Lett.* **10** 703

[54] A.A. Al-Ghamdi, O.A. Al-Hartomy, M. El Okr, A.M. Nawar, S. El-Gazzar, F. El-Tantawy, F. Yakupanoglu (2014) *Spectrochim. Acta Pt. A-Molec. Biomolec. Spectr.* **131** 512.

[55] Y.-J. Choi, H.-H. Park (2014) *J. Mater. Chem. C* **2** 98.

[56] R.S. Sreedharan, V. Ganesan, C.P. Sudarsanakumar, K. Bhavsar, R. Prabhu, V.P.P.M. Pillai (2015) *Nano Rev.* **6** 26759.

[57] S.K. Nath, N. Chowdhury, Md.A. Gafur (2015) *J. Supercond. Nov. Magn.* **28** 117.

[58] S. Karakaya, O. Ozbas (2015) *Appl. Surf. Sci.* **328** 177.

[59] Y.-J. Choi, K.-M. Kang, H.-S. Lee, H.-H. Park (2015) *J. Mater. Chem. C* **3** 8336.

[60] A.R. Deam, S.K. Muhammad (2016) *J. Appl. Phys. Sci. Int.* **7** 35.

[61] T. Jannane, M. Manoua, A. Liba, N. Fazouan, A. El Hichou, A. Almaggoussi, A. Outzourhit, M. Chaik (2017) *J. Mater. Environ. Sci.* **8** 160.

[62] A.H. Hammad, M.Sh. Abdel-wahab, S. Vattamkandathil, A.R. Ansari (2018) *Physica B* **540** 1.

[63] D.O. Samson, A.M. Ramalan, J.A. Rabba (2018) *IOSR J. Appl. Phys.* **10** PP01.

[64] O.O. Akinwunmi, O.A. Akinwumi, J.A.O. Ogundeji, A.T. Famojuro (2018) *Mater. Sci. Appl.* **9** 844.

[65] C.C. Okorieimoh, U. Chime, A.C. Nkele, A.C. Nwanya, I.G. Madiba, A.K.H. Bashir, S. Botha, P.U. Asogwa, M. Maaza, F.I. Ezema (2019) *Superlatt. Microstruct.* **130** 321.

[66] J.S. Bhat, A.S. Patil, N. Swami, B.G. Mulimani, B.R. Gayathri, N.G. Deshpande, G.H. Kim, M.S. Seo, Y.P. Lee (2010) *J. Appl. Phys.* **108** 043513.

[67] T. Prasada Rao, M.C. Santhosh Kumar (2010) *J. Alloys Comp.* **506** 788.

[68] C.-Y. Tsay, M.-C. Wang, S.-C. Chiang (2009) *J. Electron. Mater.* **38** 1962.

[69] C.-Y. Tsay, K.-S. Fan, Y.-W. Wang, C.-J. Chang, Y.-K. Tseng, C.-K. Lin (2010) *Ceram. Int.* **36** 1791.

[70] C.-Y. Tsay, K.-S. Fan, C.-Y. Chen, J.-M. Wu, C.-M. Lei (2011) *J. Electrocer.* **26** 23.

[71] S. Sali, M. Boumaour, M. Kechouane, S. Kermadi, F. Aitamar (2012) *Physica B* **407** 2626.

[72] S. Sali, M. Boumaour, S. Kermadi, A. Keffous, M. Kechouane (2012) *Superlatt. Microstruct.* **52** 438.

[73] S. Sönmezoğlu, E. Akman (2014) *Appl. Surf. Sci.* **318** 319.
[74] S.B. Qadri, H. Kim, J.S. Horwitz, D.B. Chrisey (2000) *J. Appl. Phys.* **88** 6564.
[75] Y. Cao, L. Miao, S. Tanemura, M. Tanemura, Y. Kuno, Y. Hayashi, Y. Mori (2006) *Jpn. J. Appl. Phys.* **45** 1623.
[76] H. A. Mohamed, H.M. Ali, S.H. Mohamed, M.M. Abd El-Raheem (2006) *Eur. Phys. J. Appl. Phys.* **34** 7.
[77] W. Lin, R. Ma, W. Shao, B. Liu (2007) *Appl. Surf. Sci.* **253** 5179.
[78] W. Lin, R. Ma, W. Shao, B. Kang, Z. Wu (2008) *Rare Metals* **27** 32.
[79] Y.H. Kim, K.S. Lee, T.S. Lee, B. Cheong, T.-Y. Seong, W. M Kim (2009) *Appl. Surf. Sci*. **255** 7251.
[80] T. Prasada Rao, M.C. Santhosh Kumar, A. Safarulla, V. Ganesan, S.R. Barman, C. Sanjeeviraja (2010) *Physica B* **405** 2226.
[81] R. Swapna, M.C. Santhosh Kumar (2012) *Ceram. Int.* **38** 3875.
[82] R. Swapna, M. Ashok, G. Muralidharan, M.C. Santhosh Kumar (2013) *J. Anal. Appl. Pyrol.* **102** 68.
[83] M. Jlassi, I. Sta, M. Hajji, H. Ezzaouia (2014) *Appl. Surf. Sci.* **301** 216.
[84] Dhanandjay, J. Nagaraju, S.B. Krupanidh (2008) *J. Appl. Phys.* 104 043510.
[85] G.T. Yusuf, H.O. Efunwole, M.A. Raimi, O.E. Alaje, A.K. Kazeem (2014) *J. Nucl. Phys. Mat. Sci. Radiat. Appl.* **2** 73.
[86] X.-Y. Li, H.-J. Li, Z.-J. Wang, H. Xia, Z.-Y. Xiong, J.-X. Wang, B.-C. Yang (2009) *Opt. Commun.* **282** 247.
[87] M. Caglar, S. Ilican, Y. Caglar (2009) *Thin Solid Films* **517** 5023.
[88] A. Mosbah, M.S Aida (2012) *J. Alloys Comp.* **155** 149.
[89] A. Boukhachem, B. Ouni, M. Karyaoui, A. Madani, R. Chtourou, M. Amlouk (2012) *Mater. Sci. Semicond. Process.* **15** 282.
[90] A. Jiamprasertboon, S. C. Dixon, S. Sathasivam, M.J. Powell, Y. Lu, T. Siritanon, C.J. Carmalt (2019) *ACS Appl. Electr. Mater.* **1** 1408.
[91] M. Toma, N. Ursulean, D. Marconi, A. Pop (2019) *J. Electr. Eng.* **70** 127.
[92] M.S. Abd El-Saddek, I.S. Yahia, Z.A. Alahmed, F. Yakuphanoglu (2013) *J. Electroceram.* **30** 152.
[93] D.I. Rusu, G.G. Rusu, D. Luca (2011) *Acta Phys. Pol. A* **119** 850.
[94] W.L. Liu, Y.F. Zhang (2018) *Integr. Ferroelectr.* **188** 112.
[95] M.R. Hantehzadeh, P. Salavati Dezfooli, S.A. Hoseini (2012) *J. Fusion Energy* **31** 298.
[96] M.H. Nateq, R. Ceccato, (2019) *Materials* **12** 1744.
[97] S.T. Rattanachan, P. Krongarrom, T. Fangsuwannarak (2013) *Am. J. Appl. Sci.* **10** 1427.
[98] Z. Ben Ayadi, L. El Mir, K. Djessas, S. Alaya (2009) *Thin Solid Films* **517** 6305.
[99] H. Madhdi, Z. Ben Ayadi, S. Alaya, J.L. Gauffier, K. Djessas (2014) *Superlatt. Microstruct.* **72** 60.
[100] J.C. Manifacier, J. Gasiot, J.P. Fillard (1976) *J. Phys. E: Sci. Instr.* **9** 1002.
[101] R. Swanepoel (1983) *J. Phys. E: Sci. Instrum.* **16** 1214.
[102] Sh. El Yamny, M. Abdel Rafea (2012) *J. Mod. Phys.* **2012** 1060.
[103] H.G. Hecht (1976) *J. of Research of the Nat. Bur. Stand.-A. Phys. Chem.* **80A** 567.

[104] W. Yang, Q. Li, S. Gao, J.K. Shang (2011) *Nanoscale Res. Lett.* **6** 491.

[105] A.K. Zak, A.M. Hashim, M. Darroudi (2014)*Nanoscale Res. Lett.* **9** 399.

[106] S.D. Senol, O. Ozturk, C. Terzioğlu (2015) *Ceram. Int.* **41** 11194.

[107] M.M. Mikhailov, V.V. Neshchimenko, C. Li, V.A. Vlasov (2018) *Nucl. Inst. Methods Phys. Res. B* **418** 18.

[108] L.C. Nehru, V. Swaminathan, C. Sanjeeviraja (2012) *Powder Technol.* **226** 29.

[109] C.D. Bojorge, H.R. Cánepa, U.E. Gilabert, D. Silva, E.A. Dalchiele, R.E. Marotti (2007) *J. Mater. Sci.: Mater. Electron.* **18** 1119.

[110] T. Touam, F. Boudjouan, A. Chelouche, S. Khodja, M. Dehimi, D. Djouadi, J. Solard, A. Fischer, A. Boudrioua (2015) *Optik* **126** 5548.

[111] M. Vasanthi, K. Ravichandran, N. Jabena Begum, G. Muruganantham, S. Snega, A. Panneerselvam, P. Kavitha (2013) *Superlatt. Microstruct.* **55** 180.

[112] M. Wang, E.J. Kim, S. Kim, J.S. Chung, I.-K. Yoo, E.W. Shin, S.H. Hahn, C. Park (2014) *Thin Solid Films* **516** 1124.

[113] L.B. Chandrasekar, S. Nagarajan, M. Karunakaran, T.D. Thangadurai (2019) DOI: http://dx.doi.org/10.5772/intechopen.88905.

[114] R.E. Marotti, J.A. Badán, E. Quagliata, E.A. Dalchiele (2007) *Physica B* **398** 337.

[115] C.S. Prajapati, A. Kushwaha, P.P. Sahay (2013) *J. Therm. Spray Technol.* **5** 1230.

[116] C.S. Prajapati, P.P. Sahay (2011) *Cryst. Res. Technol.* **46** 1086.

[117] S.Y. Choi, M.J. Kang, T.J. Park, R. Tap, S. Schoemaker, M. Willert-Porada (2006) *Phys. Stat. Sol. (a)* **203** R73.

[118] J.-C. Hsu, Y.-H. Lin, P.W. Wang, Y.Y. Chen (2012) *Appl. Opt.* **51** 1209.

[119] J.M. Khoshman, M.E. Kordesch (2007) *Thin Solid Films* **515** 7393.

[120] P.L. Washington, H.C. Ong, J.Y. Dai, R.P.H. Chang (1998) *Appl. Phys. Lett.* **72** 3261

[121] J.P. Zhang, G. He, L. Q. Zhu, M. Liu, S.S. Pan, L.D. Zhang (2007) *Appl. Surf. Sci.* **253** 9414.

[122] Sh. Chen, Q. Li, I. Ferguson, T. Lin, L. Wan, Zh.Ch. Feng, L. Zhu, Zh. Ye (2017) *Appl. Surf. Sci.* **421** 383.

[123] P. Janicek, K.M. Niang, J. Mistrik, K. Palka, A.J. Flewitt (2017) *Appl. Surf. Sci.* **421** 557.

[124] L. Miao, S. Tanemura, L. Zhao, X. Xiao, X.T. Zhang (2013) *Thin Solid Films* **543** 125.

[125] C.-H. Zhai, R.-J. Zhang, X. Chen, Y.-X. Zheng, S.-Y. Wang, J. Liu, N. Dai, L.-Y. Chen (2016) *Nanoscale Res. Lett.* **11** 407.

[126] N. Ehrmann, R. Reineke-Koch (2010) *Thin Solid Films* **519** 1475.

[127] S.-D. Yang, Y.-X. Zheng, L. Yang, Z.-H. Liu, W.-J. Zhou, S.-Y. Wang, R.-J. Zhang, L.-Y. Chen (2017) *Appl. Surf. Sci.* **421** 891.

[128] J. Tauc, R. Grigorovici, A. Vancu (1966) *Phys. Stat. Sol.* **15** 627.

[129] J.I. Cisneros (1998) *Appl. Opt.* **37** 5262.

[130] A. Tejada, L. Montañez, C. Torres, P. Llontop, L. Flores, F. De Zela, A. Winnacker, J.A. Guerra (2019) *Appl. Opt.* **58** 9585.

[131] W.C. Wang, M. Badylevich, V.V. Afanas'ev, A. Stesmans, M. Popovici, K. Tomida, N. Menou, J.A. Kittl, M. Lukosius, C. Baristiran Kaynak, Ch. Wenger (2011) *Thin Solid Films* **519** 5730.

[132] G.D. Cody, B.G. Brooks, B. Abeles (1982) *Sol. Energy Mater.* **8** 231.

[133] A.S. Ferlauto, G.M. Ferreira, J.M. Pearce, C.R. Wronski, R.W. Collins, X. Deng, G. Ganguly (2002) *J. Appl. Phys.* **92** 2424.

[134] P.Y.Yu, M. Cardona (2010) *Fundamentals of Semiconductors. Physics and Materials Properties*, 4th Edition, Springer, pp. 254-273.

[135] J. Aarik, H. Mändar, M. Kirm, L. Pung (2004) *Thin Solid Films* **466** 41.

[136] H. Tang, K. Prasad, R. Sanjinès, P.E. Schmid, F. Lévy (1994) *J. Appl. Phys.* **75** 2042.

[137] S. Tanemura, L. Miao, P. Jin, K. Kaneko, A. Terai, N Nabatova-Gabain (2003) *Appl. Surf. Sci.* **212-213** 654.

[138] T. Arroval, L. Aarik, R. Rammula, V. Kruusla, J. Aarik (2016) *Thin Solid Films* **600** 119.

[139] L. Aarik, T. Arroval, H. Mändar, R. Rammula, J. Aarik (2020) *Appl. Surf. Sci.* **530** 147229.

[140] I.H. Malitson (1965) *J. Opt. Soc. Am.* **55** 1205.

[141] A. Kasikov, A. Tarre, M. Marandi (2019) *J. of Electr. Eng.* **70** 36.

[142] S. Lee, J. Hong (2000) *Jap. J. Appl. Phys.* **39** Part 1 241.

[143] R. Henríquez, P. Grez, E. Muñoz, H. Gómez, J.A. Badán, R.E. Marotti, E.A. Dalchiele (2010) *Thin Solid Films* **518** 1774.

[144] A.S. Hassanien, A.A. Akl (2020) *Physica B* **576** 411718.

[145] W.M. Yim (1971) *J. Appl. Phys.* **42** 2854.

[146] T. Wang, B. Daiber, J.M. Frost, S.A. Mann, E.C. Garnett, A. Walsh, B. Ehrler (2017) *Energy Environ. Sci.* **10** 509.